Special Feature: Power Electronics for Hybrid Vehicles

Research Report

Analysis and Design of Multiport DC/DC Converter for Next-generation Hybrid-vehicle Subsystems

Kenichi Itoh, Shuntaro Inoue, Masanori Ishigaki, Takahide Sugiyama and Takaji Umeno

Report received on May 11, 2017

ABSTRACT A multiport converter using a coupling inductor and a hybrid modulation technique is proposed for dual-voltage 12 V/48 V hybrid-vehicle (HV) subsystems. The converter integrates two circuit topologies: an isolated DC/DC converter (dual active bridge) and a non-isolated multi-phase DC/DC converter. The new HV subsystem can be constructed using a multiport converter without additional circuit components. This paper describes the method for integrating the two circuit topologies and the operation principle and inductance behavior of the magnetic components. To validate the converter performance, a 1.0-kW, 50-kHz prototype was constructed and tested. The experimental waveforms showed the parallel operation of two topologies in one circuit, and high efficiencies of over 90% were measured over a wide output power range, with a maximum efficiency of 96.5%.

KEYWORDS Multiport, DC Conversion, Bridge Circuit, 48V, Hybrid Vehicle

1. Introduction

Hybrid electric vehicles (HVs) are becoming mainstream as a result of performance improvements of storage devices such as Ni-H and Li-ion batteries. Additionally, more electricity-intense vehicles, such as plug-in HVs, purely electric vehicles, and fuel-cell vehicles, are being launched, and these vehicles require more batteries and higher power conversion to achieve a long cruising range. Subsystems for HVs typically use 12-V DC bus voltage and lead-acid batteries. However, the load in the 12-V DC subsystem is rapidly increasing because these vehicles need more electricity for sensors, actuators, relay switches, displays, and microprocessing units (MPUs). Thus, the 12-V DC wire harness is already being operated near its current rating.[1, 2] In the near future, more sensors and MPUs will be needed for developing intelligent transport systems and self-driving cars. It is therefore important to mitigate current stress in the 12-V DC subsystem for realizing a more sophisticated automotive system. The 48-V DC drive system has been developed for mild hybridization of conventional cars. Heavier load components operate at 48-V DC, current stress on the 12-V DC subsystem can be decreased, and the cable cross section is expected to become smaller. The 48-V DC bus is also a promising technology to mitigate the load current for HVs. **Figure 1** shows a dual-voltage HV subsystem design with the existing 12-V DC bus and the new 48-V DC bus. In Fig. 1(a), the system is constructed with conventional converters. An isolated DC/DC converter is connected to maintain galvanic isolation between the high-voltage main battery (generally, over 200 V DC) and the 48-V system. Additionally, a non-isolated DC/DC converter is needed to convert the 48-V DC

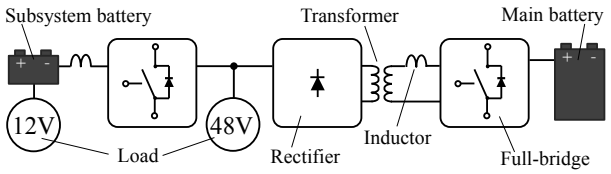

(a) System using conventional DC/DC converters. The full bridge has four switching devices, and the rectifier has two or four diodes.

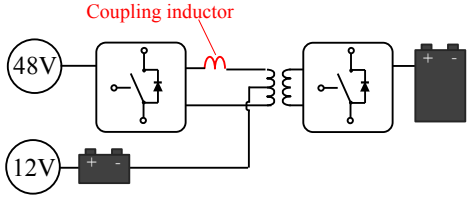

(b) System using the proposed multiport converter. The new design dispenses with the rectifier and an inductor.

Fig. 1 Dual-voltage 12 V/48 V HV subsystem topologies.

bus to 12 V DC. This arrangement decreases the current stress in the 12-V DC bus. However, the two converters need at least ten semiconductor devices and three magnetic components.

A multiport DC/DC converter has been proposed to reduce the size and cost of power conversion system by saving circuit components.[3-5] We also proposed a multiport converter using a coupling inductor and hybrid-modulation technique.[6] Figure 1(b) shows the dual-voltage subsystem using our multiport converter. The number of components can be reduced with respect to the conventional two-converter system, that is, to eight semiconductor devices and two magnetic converters (instead of ten and three, respectively). Our converter is suitable for realizing a dual-voltage HV subsystem with a compact size and low cost.

This paper describes the integration technique and design of the multiport converter. Section 2 describes the operation principle. In Sec. 3, the prototype design is presented. Section 4 presents the validation of the principle and discusses experimental results.

2. Operation Principle

2. 1 Conventional Circuit Operation

Figure 2 shows the conventional circuits used in the dual-voltage subsystem of Fig. 1(a), and its waveforms are shown in **Fig. 3**. A non-isolated multi-phase DC/DC converter is shown in Fig. 2(a).[7] The converter has a coupling inductor, and its windings (L_u, L_v) are coupled directly with a coupling coefficient k_L. Figure 3(a) shows the ideal waveforms for the multi-phase DC/DC converter. The first derivatives of the inductor current i_u and the output current i_C can be expressed as follows:

$$\frac{di_u}{d\theta} = \frac{v_u - k_L \cdot v_v}{\omega_{sw}(1-{k_L}^2)L_u}, \quad (1)$$

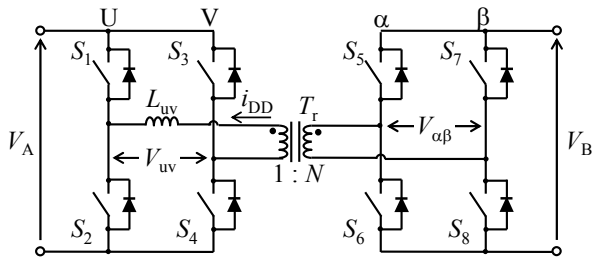

(a) Non-isolated multi-phase DC/DC converter.

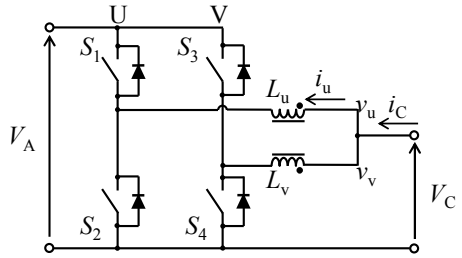

(b) Dual active bridge (DAB) isolated converter.

Fig. 2 Schematics of conventional DC/DC converters.

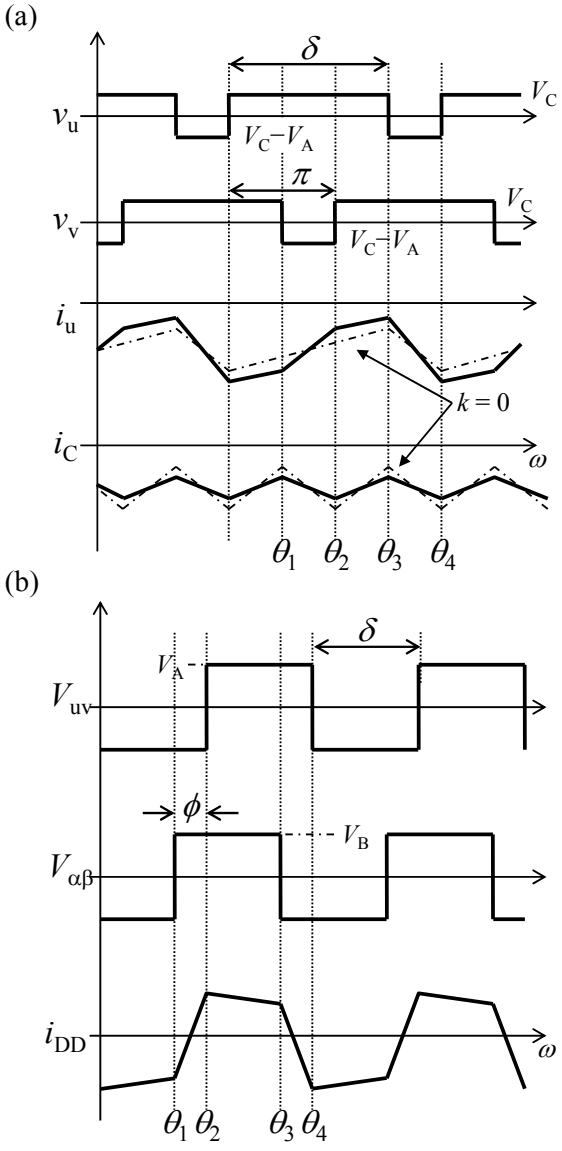

Fig. 3 Ideal waveforms for conventional DC/DC converters: (a) multi-phase converter in Fig. 2(a) and (b) DAB in Fig. 2(b).

$$\frac{di_u}{d\theta} = \frac{v_u + v_v}{\omega_{sw}(1+k_L)L_u}, \quad (2)$$

$$\begin{aligned} v_u &= V_C, \quad v_v = V_C - V_A && [\theta_1 < \theta < \theta_2], \\ v_u &= V_C, \quad v_v = V_C && [\theta_2 < \theta < \theta_3], \\ v_u &= V_C - V_A, \quad v_v = V_C && [\theta_3 < \theta < \theta_4], \end{aligned}$$

where v_u and v_v are the voltages applied to the two windings of the coupling inductor, and ω_{sw} (= $2\pi f_{sw}$) is the switching frequency. The output voltage V_C can be controlled by the duty ratio δ as follows:

$$V_C = V_A\left(1 - \frac{\delta}{2\pi}\right). \quad (3)$$

Figure 2(b) shows an isolated DC/DC converter (DAB), and its waveforms for a duty ratio $\delta = \pi$ are shown in Fig. 3(b).[8-10] The DAB has two full bridges, and the windings of transformer T_r are connected to the bridge middle points. An inductor is also connected between the middle point and the transformer winding to design power rating of the DAB. The first derivative of the inductor current i_{DD} is given by:

$$\frac{di_{DD}}{d\theta} = \frac{V_{\alpha\beta}/N - V_{uv}}{L_{eq,DAB}}, \quad (4)$$

$$\begin{aligned} V_{uv} &= -V_A, \; V_{\alpha\beta} = V_B/N && [\theta_1 < \theta < \theta_2], \\ V_{uv} &= V_A, \quad V_{\alpha\beta} = V_B/N && [\theta_2 < \theta < \theta_3], \\ V_{uv} &= V_A, \quad V_{\alpha\beta} = -V_B/N && [\theta_3 < \theta < \theta_4], \end{aligned}$$

where V_{uv} and $V_{\alpha\beta}$ are the transformer terminal voltages of primary and secondary windings, respectively, and N is the turn ratio of the transformer. L_{eq} is the equivalent inductance for DAB operation:

$$L_{eq,DAB} = L_{uv} + L_l, \quad (5)$$

where L_l is the primary referenced leakage inductance of the transformer. The isolated power P_{DD} is controlled by adjusting the phase angle difference ϕ between the primary and secondary full bridges, and P_{DD} is given as follows:

$$P_{DD} = \frac{V_A \cdot V_B/N}{\pi\omega_{sw}L_{eq,DAB}}\phi(\pi - \phi). \quad (6)$$

2. 2 Proposed Multiport Converter

Figure 4 shows a schematic of the proposed multiport converter. This converter has a transformer T_r and a coupling inductor L_{uv}, and their windings are connected to the middle points of the primary and secondary full bridges. The transformer has a center tap on the primary side, which provides an extra DC port. When the two topologies in Fig. 2 are integrated, the primary full bridge and coupling inductor are shared. The converter has three DC ports in one circuit, referred to as Port A, Port B and Port C. The multi-phase DC/DC converter operates between Port A and Port C, and the Port C output voltage V_C is controlled by adjusting the duty ratio δ. The DAB converter also operates between Port A and Port B, and its isolated power P_{DD} is controlled by adjusting the phase angle difference ϕ. Hence, two topologies with different output voltages (power) can be controlled simultaneously because of the different modulation parameters.

Figure 5 shows the details of the magnetic components and current flow for each topology. In Fig. 5(a), the output current into Port C passes through the windings by way of a center tap during multi-phase converter operation. The flux is cancelled in the transformer core, and the coupling inductor has a high inductance of $L \sim (1 + k_L)$ against the common mode current. This high inductance

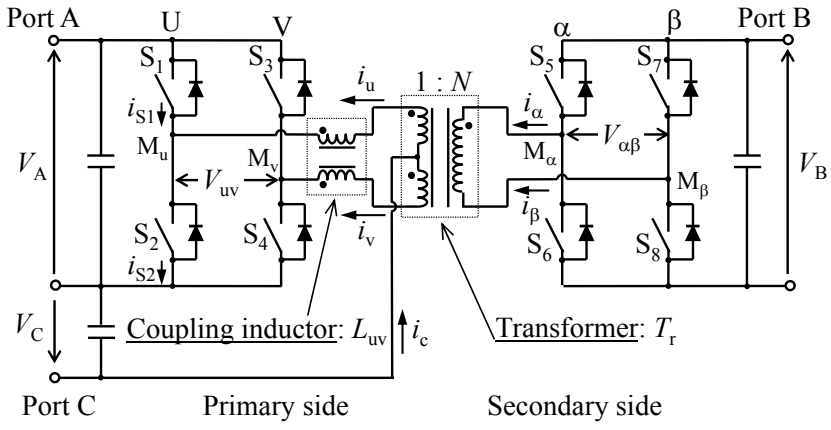

Fig. 4 Proposed multiport converter. The primary full bridge and a coupling inductor are shared by two circuit topologies. DC power is transferred mutually between three DC ports in one circuit.

value is suitable for decreasing ripples in the output current i_C. On the other hand, during DAB operation in Fig. 5(b), both the excitation and load currents pass through the windings, and the coupling inductor has a low inductance of $L \sim (1-k_L)$ against the differential mode current. Since the isolated power P_{DD} is inversely proportional to L_{eq} (Eq. (6)), this low inductance value is suitable for achieving a high power rating for the DAB. The two topologies can be integrated without additional magnetic components because each current mode has a different inductance value.

Figure 6 shows the ideal waveforms when DC power is transferred from Port B to both Port A and Port C. The differential mode current i_{DD} and the common mode current i_C are given by $i_{DD} = (i_u - i_v)/2$ and $i_C = i_u + i_v$, respectively. The secondary winding current i_α is equal to i_{DD}/N. The primary inductor current i_u contains a common mode current waveform because of multi-phase converter operation, and i_u is given by $i_u = i_{DD} + i_C/2$. **Figure 7** shows the equivalent circuits and current flow gradients on the primary side. The state of the circuit and the i_{DD} formula are described for one half period as follows:

Mode I [$\theta_1 < \theta < \theta_2$]: At θ_1, S_5 is turned on, and the state of S_2, S_4 and S_8 is on. The transformer is excited, and the differential mode current i_{DD} begins to increase as a result of the voltage V_B/N:

$$i_{DD}(\theta) = \frac{V_B / N}{\omega_{sw} L_{eq}} \cdot \theta + i_{DD}(0), \tag{7}$$

where $i_{DD}(0)$ is the initial current at θ_1 ($i_{DD}(0)$ is not equal to zero in the non-ideal condition of $NV_A/V_B \neq 1$). Then, the inductor current i_u is increased by the resulting voltage $V_C + V_B/2N$, and the current i_v is decreased by the resulting voltage $V_C - V_B/2N$.

Mode II [$\theta_2 < \theta < \theta_3$]: At θ_2, S_2 is turned off, and the state of S_1 becomes on. i_{DD} is changed by the resulting voltage $V_B/N - V_A$:

$$i_{DD}(\theta) = \frac{V_B / N - V_A}{\omega_{sw} L_{eq}} \cdot (\theta - \phi) + i_{DD}(\phi). \tag{8}$$

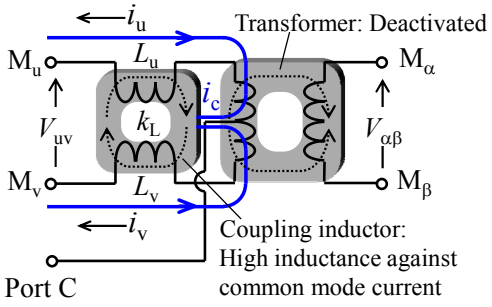

(a) Multi-phase DC/DC converter function

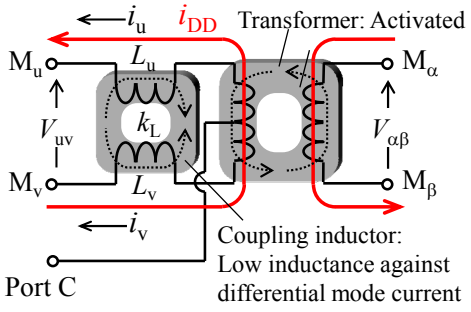

(b) DAB converter function

Fig. 5 Current path and inductance behavior of magnetic components. The two magnetic components show different inductance values for each current mode (common mode and differential mode).

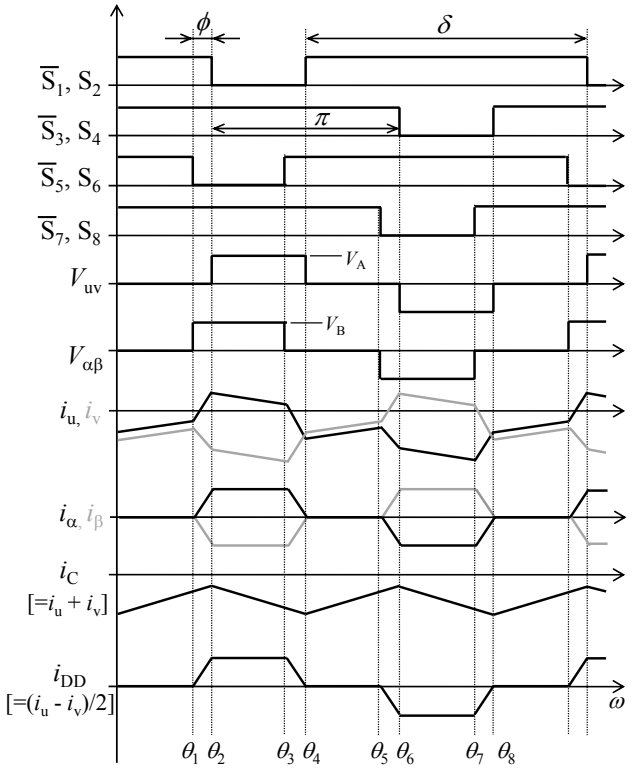

Fig. 6 Ideal waveforms for multiport converter. The voltage ratio $NV_A/V_B = 1$, and losses and dead time are ignored.

In the ideal condition, i_{DD} remains unchanged because $V_B/N - V_A = 0$. Then, the current i_u begins to decrease due to the resulting voltage $V_C + V_B/2N - V_A$, and the current i_v continues to decrease due to the voltage $V_C - V_B/2N$.

Mode III [$\theta_3 < \theta < \theta_4$]: At θ_3, S_5 is turned off. The excitation period ends, and i_{DD} begins to decrease as a result of the voltage $-V_A$:

$$i_{DD}(\theta) = \frac{-V_A}{\omega_{sw} L_{eq}} \cdot \{\theta - (2\pi - \delta)\} + i_{DD}(2\pi - \delta). \quad (9)$$

Then, i_u continues to decrease due to the resulting voltage $V_C - V_A$, and i_v increases due to the resulting voltage V_C.

Mode IV [$\theta_4 < \theta < \theta_5$]: At θ_4, S_2 is turned on. i_{DD} remains unchanged:

$$i_{DD}(\theta) = i_{DD}(2\pi - \delta + \phi). \quad (10)$$

Then, i_u and i_v increase due to the resulting voltage V_C.

Here, the boundary condition is $i_{DD}(0) = [-i_{DD}(\pi)]$ at θ_5. The initial current $i_{DD}(0)$ is calculated as follows:

$$i_{DD}(0) = \frac{V_A - V_B/N}{4\omega_{sw} L_{eq}}(2\pi - \delta). \quad (11)$$

The Port A average output current $i_{out,avg}$ can be calculated by integration of i_{DD} from θ_1 to θ_3:

$$i_{out,avg} = \frac{2}{\pi}\int_{\theta 1}^{\theta 3} i_{DD}(\theta) \cdot d\theta = \frac{V_B/N}{\pi\omega_{sw} L_{eq}} \phi(2\pi - \delta - \phi/2). \quad (12)$$

The isolated power P_{DD} is given by $P_{DD} = V_A \times i_{out,avg}$. In Eq. (12), P_{DD} is dependent on both δ and ϕ. The duty ratio δ is kept at a constant value in steady-state operation. Thus, the isolated power P_{DD} is controlled only by phase angle ϕ.

3. Prototype Design

To validate the operation principle and circuit

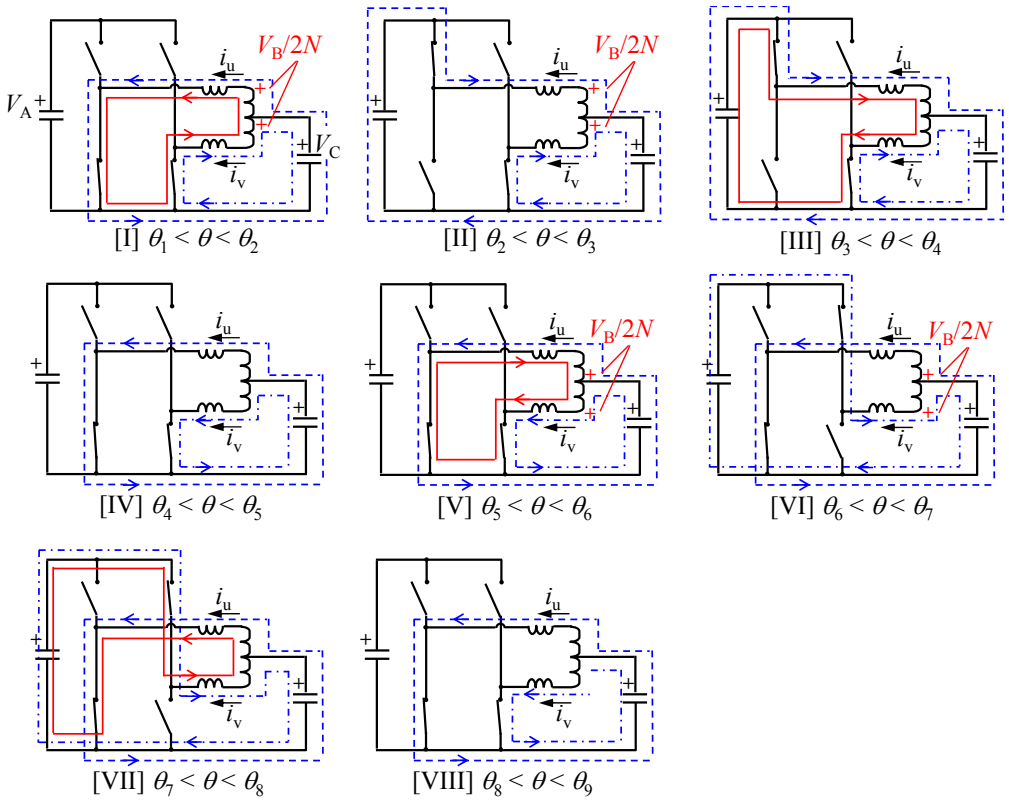

Fig. 7 Equivalent circuit for primary side full bridge. The output voltage V_B/N appears in modes I, II, V and VI.

performance, a 1.0-kW, 50-kHz prototype was constructed (**Fig. 8**). The experimental circuit is depicted in **Fig. 9**, and its circuit parameters are summarized in **Table 1**.

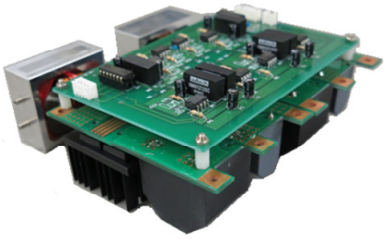

Fig. 8 Photograph of prototype.

3. 1 Magnetic Components

A Mn-Zn ferrite core (TDK, PC95PQ50/50) was employed for the transformer core. The transformer turn ratio was $N = 4$, and the number of turns for the primary and secondary windings was $n_{11} = n_{12} = 2$ and $n_2 = 8$, respectively. The transformer core had no air gap, and the measured primary magnetizing inductance and coupling coefficient were $L_{Tr1} = 55$ μH and $k_{Tr} = 0.999$, respectively. The coupling inductor was designed using the same core as the transformer, but with an air gap of 0.5 mm total. The inductor turn number was $n_u = n_v = 2$, and the measured self-inductance and coupling coefficient were $L_u = L_v = 3.5$ μH and $k_L = 0.94$, respectively.

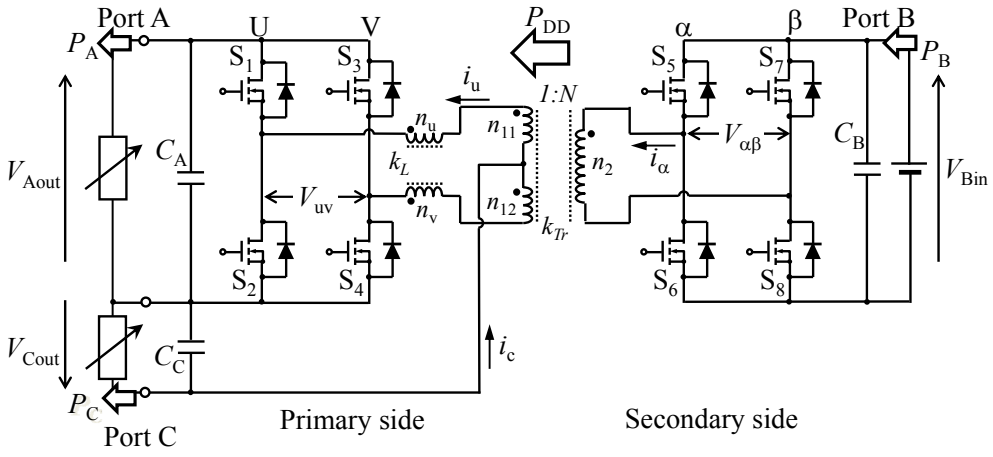

Fig. 9 Experimental circuit configuration.

Table 1 Experimental circuit configuration.

Switching frequency	f_{sw}	50 kHz
Rated power	P_{DD_MAX}	1.0 kW
Rated Voltage	V_{Aout}, V_{Bin}, V_{Cout}	48 V, 200 V, 12 V
Turn number of transformer	n_{11}, n_{12}, n_2	1, 1, 8
Turn ratio of transformer	N	4
Magnetizing inductance of transformer [Primary]	L_{Tr1}	55 μH
Coupling coefficient of transformer	k_{Tr}	0.999
Turn number of inductor	n_u, n_v	2, 2
Self inductance of inductor	L_u, L_v	3.5 μH
Coupling coefficient of inductor.	k_L	0.94
Primary Si MOSFETs	S_1 - S_4	IRFP4568
Secondary Si MOSFETs	S_5 - S_8	2SK3681
Dead time	T_d	200 ns

3. 2 Power Semiconductor Devices

150-V Si MOSFETs (Infineon, IRFP4568) were employed as the primary full-bridge due to their low on-resistance and fast switching. 650-V Si MOSFETs (Fuji-electric, 2SK3681) were employed as the secondary full bridge. All switches were connected to a two-layer power-stage circuit board with a 200-μm copper pattern. A gate-drive circuit board was connected to the power-stage board on the upper side, and the optical gate drive used integrated circuits (Avago, HCPL-3120) with a gate voltage V_G = 15 V.

3. 3 Controller

A digital signal processor calculated δ and ϕ to control the output voltage (power), while the modulation was implemented in a field-programmable gate array. **Figure 10** shows the control diagram for the multiport converter. The output voltage V_{Aout} was command-controlled to V_A* = 48 V by adjusting ϕ with proportional-integral (PI) feedback. In addition, the output voltage V_{Cout} was command-controlled to V_C* = 12 V by adjusting δ with PI feedback and a feedforward of $\delta_{ff} = 2\pi\,(1 - V_C*/V_A)$. Secondary carriers were shifted by ϕ, and gate signals were generated by comparing carriers and the duty ratio δ.

4. Experimental Results and Discussion

As shown in Fig. 9, a DC power supply was connected to Port B, and the input voltage was set to V_{Bin} = 200 V. The output voltages were kept constant at V_{Aout} = 48 V and V_{Cout} = 12 V. Electrical loads were connected to Port A and Port C. The transformer terminal voltages V_{uv} and $V_{\alpha\beta}$ and inductor current i_u were measured using an oscilloscope (Tektronix, DPO4034). The efficiency of the prototype was evaluated using a power scope (Yokogawa, PX-8000). The input and output DC currents at each Port were measured using pull-through current sensors (Hioki, CT6862 and CT6863).

Figure 11 shows the measured voltage and current waveforms at P_{DD} = 1000 W. In Fig. 11(a), the converter delivers DC power from Port B to Port A (P_A = 1000 W, P_C = 0 W). The measured output voltages were V_{Aout} = 48 V and V_{Cout} = 12 V, and the duty ratio δ and phase angle ϕ were adjusted to $\delta = 75\%*2\pi$ and $\phi = 3\%*2\pi$ (= 9.4 deg). The inductor current i_u has no DC current offset because P_C = 0 W. On the other hand, the converter delivers DC power from Port B to Port C (P_A = 0 W,

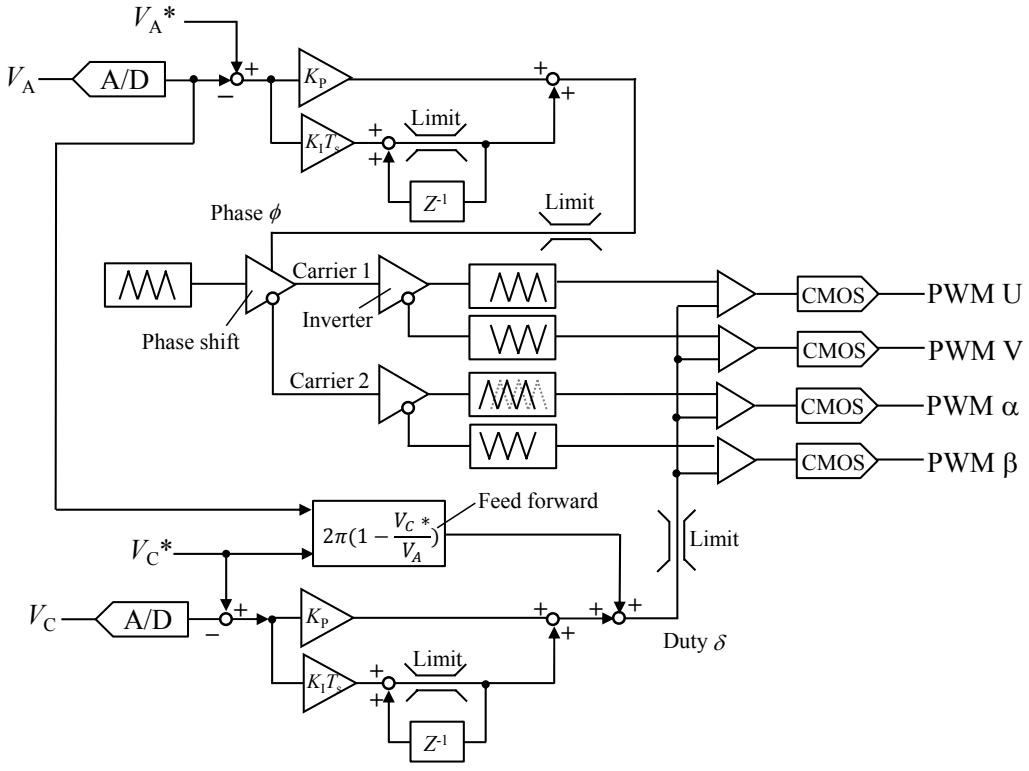

Fig. 10 Block diagram of converter PI controller.

P_C = 1000 W) in Fig. 11(b). To maintain V_C = 12 V, the multi-phase converter delivers DC power to Port C. The inductor current i_u is shifted by $i_C/2$ (= $P_C/2V_C$ ≅ 40 A). The output voltages V_{Aout} and V_{Cout} are maintained at 48 V and 12 V, respectively.

Figure 12(a) shows the efficiency and loss as a function of P_A. The maximum efficiency of 95.6% was measured at P_A = 400 W, and efficiencies of 90% were measured over a wide range of output power P_A above 100 W. Figure 12(b) shows the efficiency and loss as a function of P_C. Since a high DC current passes through the windings and switches, the conduction loss and copper loss were large. Thus, the loss in Fig. 12(b) is higher than that in Fig. 12(a). The maximum efficiency of 94% was measured at P_C = 325 W.

5. Conclusion

A multiport converter using a coupling inductor and a hybrid modulation technique was proposed for dual-voltage 12 V/48 V HV subsystems. An isolated DC/DC converter and a non-isolated DC/DC converter were integrated, and the new subsystem was constructed with one circuit. This paper described the operation principle and design of the multiport converter. To demonstrate its performance, a 1.0-kW, 50-kHz prototype was constructed and tested. The two topologies were controlled simultaneously using the duty ratio and phase angle difference, and constant output voltages of 12 V and 48 V were measured in steady-state operation. The prototype achieved a high efficiency of more than 90% over a wide output range, with a maximum efficiency of 95.6%. Our multiport converter was an attempt to realize a dual-voltage HV subsystem with compact size, low cost, and high efficiency.

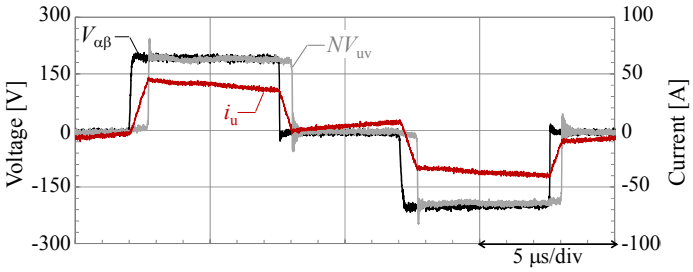

(a) Port B to Port A, P_A = 1000 W

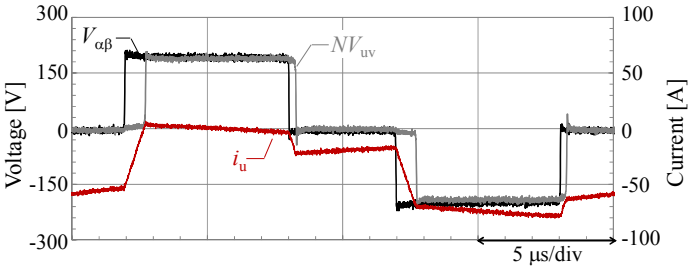

(b) Port B to Port C, P_C = 1000 W

Fig. 11 Experimental transformer terminal voltage waveforms and inductor current waveforms.

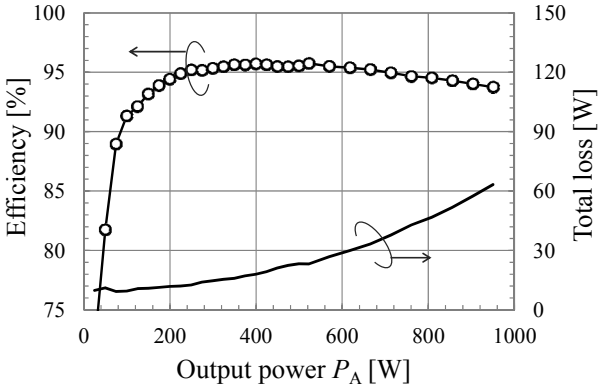

(a) Port B (200 V) to Port A (48 V)

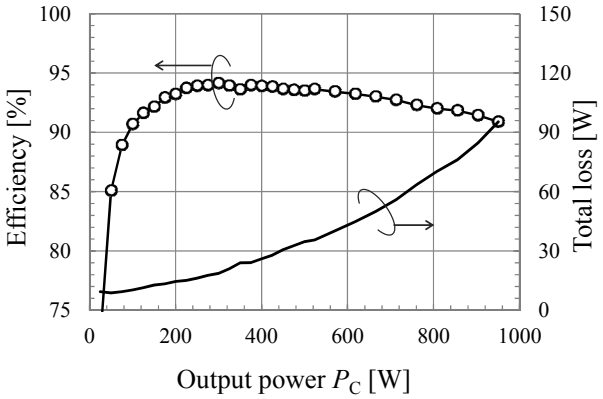

(b) Port B (200 V) to Port C (12 V)

Fig. 12 Measured efficiencies and losses.

References

(1) Kassakian, J. G., "Automotive Electrical Systems—the Power Electronics Market of the Future", *IEEE Appl. Power Electron. Conf. Expos. (APEC)*, (2000), No. 6521757.
(2) Teratani, T., "Impact of DC48V on Automotive Power Supply Systems—Comparison with DC42V and Future View under DC60V", *IEEJ Trans. Ind. Appl.*, Vol. 135, No. 9 (2015), pp. 892-897.
(3) Tao, H. et al., "Multiport Converters for Hybrid Power Sources", *IEEE Power Electron. Specialists Conf.* (2008), pp. 3412-3418.
(4) Zhang, Z. et al., "Analysis and Design of a Bidirectional Isolated DC-DC Converter for Fuel Cells and Supercapacitors Hybrid System", *IEEE Trans. Power Electron.*, Vol. 27, No. 2 (2012), pp. 848-859.
(5) Zhao, C. et al., "An Isolated Three-port Bidirectional DC-DC Converter with Decoupled Power Flow Management", *IEEE Trans. Power Electron.*, Vol. 23, No. 5 (2008), pp. 2443-2453.
(6) Ishigaki, M. et al., "A New Isolated Multi-port Converter Using Interleaving and Magnetic Coupling Inductor Technologies", *Appl. Power Electron. Conf. Expos. (APEC)* (2013), No. 13530196.
(7) Wong, P. et al., "Performance Improvements of Interleaving VRMs with Coupling Inductors", *IEEE Trans. Power Electron.*, Vol. 16, No. 4 (2001), pp. 499-507.
(8) De Doncker, R. W. A. A. et al., "A Three-phase Soft Switched High-power-density DC/DC Converter for High Power Applications", *IEEE Trans. Ind. Appl.*, Vol. 27, No. 1 (1991), pp. 63-73.
(9) Krismer, F. and Kolar, J. W., "Accurate Power Loss Model Derivation of a High-current Dual Active Bridge Converter for an Automotive Application", *IEEE Trans. Ind. Electron.*, Vol. 57, No. 3 (2010), pp. 881-891.
(10) Inoue, S. and Akagi, H., "A Bidirectional Isolated DC–DC Converter as a Core Circuit of the Next-generation Medium-voltage Power Conversion System", *IEEE Trans. Power Electron.*, Vol. 22, No. 2 (2007), pp. 535-542.

Kenichi Itoh
Research Field:
- Power Electronics
Academic Societies:
- The Institute of Electrical Engineers of Japan
- IEEE

Shuntaro Inoue
Research Field:
- Power Electronics
Academic Societies:
- The Institute of Electrical Engineers of Japan
- The Japan Society of Mechanical Engineers

Masanori Ishigaki
Research Fields:
- Power Electronics
- HV/EV Electric Drive System
Academic Society:
- The Institute of Electrical Engineers of Japan
Awards:
- IEEJ Best Presentation Award, 2007, 2012
- IEEE IPEC Second Paper Award, 2010
- IEEE APEC Outstanding Presentation Award, 2012
- IEEJ Encouraging Prize Award, 2012

Takahide Sugiyama
Research Fields:
- Power Device
- Device Simulation
- Defects in Semiconductor
Academic Society:
- The Japan Society of Applied Physics

Takaji Umeno
Research Fields:
- Power Electronics
- HV/EV Electric Drive System
Academic Degree: Dr.Eng.
Academic Societies:
- IEEE
- The Institute of Electrical Engineers of Japan
- The Society of Instrument and Control Engineers
- The Society of Automotive Engineers of Japan
Awards:
- IEEE/IES Outstanding Paper Award, 1994
- Robomec '94 Best Paper Award, 1995
- R&D 100 Award, 1997
- SICE Chubu Chapter Award for Outstanding Technology, 2002
- Paper Award of AVEC '02, 2002